ORGANIC LETTERS

2011
Vol. 13, No. 17
4644–4647

Synthesis of Large Polycyclic Aromatic Hydrocarbons from Bis(biaryl)acetylenes: Large Planar PAHs with Low π-Sextets

Tse-An Chen and Rai-Shung Liu*

Department of Chemistry, National Tsing-Hua University, No. 101, Section 2, Kuang-Fu Road, Hsinchu, Taiwan, 30013, R. O. C.

rsliu@mx.nthu.edu.tw

Received July 11, 2011

ABSTRACT

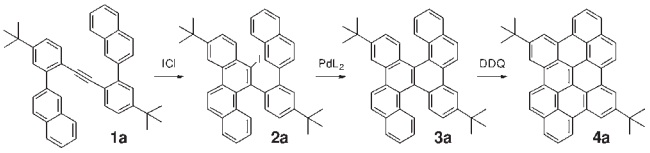

A new synthesis of large PAHs with low Clar sextets was developed. This synthesis involves initial bis(biaryl)acetylene 1, which undergoes initial ICl-aromatization and a subsequent Mizoroki–Heck coupling reaction to give dibenzochrysene derivative 3 that can be transformed into planar PAHs 4 using DDQ-oxidation.

Scholl oxidation of the 1,2-diphenylbenzene units is a powerful tool to access large polycyclic aromatic hydrocarbons (PAHs).[1] Due to the fully populated Clar π-sextets,[2] the reported large PAHs such as **I**–**III** (Scheme 1) typically have irreducible highest occupied molecular orbital and lowest unoccupied molecular orbital (HOMO–LUMO) energy gaps.[3] To seek large PAHs with low Clar π-sextets,[4] we reported the use of bis(biaryl)diynes **IV** for short syntheses of PAHs **VI** and their heavier congeners,[5] as depicted in Scheme 1. Nevertheless, these PAHs have nonplanar geometries because of the steric interactions around the two cove regions. We envisage that planar PAHs will be beneficial for organic optoelectronic devices due to their strong intermolecular $\pi-\pi$ interactions.[6]

Previously, we reported the synthesis of dibenzochrysenes[7,8] based on the 2-fold aromatizations of bis(biaryl)acetylenes.[8] Here, we report further development of this method to achieve the synthesis of planar PAHs **4a**–**4e** with low Clar π-sextets in Figure 1; PAHs **4b** and **4c** are structurally related to the parent skeleton **4a** with two additional benzenes, whereas PAHs **4d** and **4e** have four extra benzenes. An examination of their photophysical properties with increasing benzene arrays is the focus of this investigation.

As depicted in Scheme 2, treatment of bis(biaryl)acetylene **1a** with ICl (1.1 equiv) in cold dichloromethane (DCE, −78 °C, 3 h) afforded iodo derivative **2a** in 82% yield. A subsequent Mizoroki–Heck coupling reaction of species **2a** provided a large dibenzochrysene derivative **3a**

(1) (a) Wu, J.; Pisula, W.; Müllen, K. *Chem. Rev.* **2007**, *107*, 718. (b) Watson, M. D.; Fechtenkötter, A.; Müllen, K. *Chem. Rev.* **2001**, *101*, 1267. (c) Müllen, M.; Kübel, C.; Müllen, K. *Chem.—Eur. J.* **1998**, *4*, 2099. (d) Feng, X.; Pisula, W.; Müllen, K. *Pure. Appl. Chem.* **2009**, *81*, 2203.

(2) (a) Clar, E. *The Aromatic Sextet*; Wiley: New York, 1972. (b) Clar, E. *Polycyclic Hydrocarbons*, Vols. 1 and 2; Academic Press: London, 1964.

(3) (a) Böhme, T.; Simpson, C. D.; Müllen, K.; Rabe, J. P. *Chem.—Eur. J.* **2007**, *13*, 7349. (b) Feng, X.; Wu, J.; Ai, M.; Pisula, W.; Zhi, L.; Rabe, J. P.; Müllen, K. *Angew. Chem., Int. Ed.* **2007**, *46*, 3033. (c) Dötz, F.; Brand, J. D.; Ito, S.; Gherghel, L.; Müllen, K. *J. Am. Chem. Soc.* **2000**, *122*, 7707.

(4) (a) Wu, T. C.; Chen, C. H.; Hibi, D.; Shimizu, A.; Tobe, Y.; Wu, Y. T. *Angew. Chem., Int. Ed.* **2010**, *49*, 7059. (b) Zhang, X.; Jiang, X.; Zhang, K.; Mao, L.; Luo, J.; Chi, C.; Chan, H. S. O.; Wu, J. *J. Org. Chem.* **2010**, *75*, 8069. (c) Criado, A.; Peña, D.; Cobas, A.; Guitián, E. *Chem.—Eur. J.* **2010**, *16*, 9736.

(5) Chen, T. A.; Liu, R. S. *Chem.—Eur. J.* **2011**, *17*, 8023.

(6) (a) Schmidt-Mende, L.; Fechtenkötter, A.; Müllen, K.; Moons, E.; Friend, R. H.; Mackenzie, J. D. *Science* **2001**, *293*, 1119. (b) Bendikov, M.; Wudl, F. *Chem. Rev.* **2004**, *104*, 4891. (c) Anthony, J. E. *Angew. Chem., Int. Ed.* **2008**, *47*, 452. (d) Jäckel, F.; Watson, M. D.; Müllen, K.; Rabe, J. P. *Phys. Rev. Lett.* **2004**, *92*, 188303.

(7) (a) Yamaguchi, S.; Swager, T. M. *J. Am. Chem. Soc.* **2001**, *123*, 12087. (b) Kumar, S.; Varshney, S. K. *Mol. Cryst. Liq. Cryst.* **2002**, *378*, 59. (c) Navale, T. S.; Thakur, K.; Rathore, R. *Org. Lett.* **2011**, *13*, 1634. (d) Schultz, A.; Laschat, S.; Diele, S.; Nimtz, M. *Eur. J. Org. Chem.* **2003**, 2829.

(8) (a) Li, C. W.; Wang, C. I.; Liao, H. Y.; Chaudhuri, R.; Liu, R. S. *J. Org. Chem.* **2007**, *72*, 9203. (b) Chaudhuri, R.; Hsu, M. Y.; Li, C. W.; Wang, C. I; Chen, C. J.; Lai, C. K.; Chen, L. Y.; Liu, S. H.; Wu, C. C.; Liu, R. S. *Org. Lett.* **2008**, *10*, 3053.

10.1021/ol201854g
Published on Web 08/09/2011

Scheme 1. All Benzenoid PAHs and Low Clar Sextets PAHs

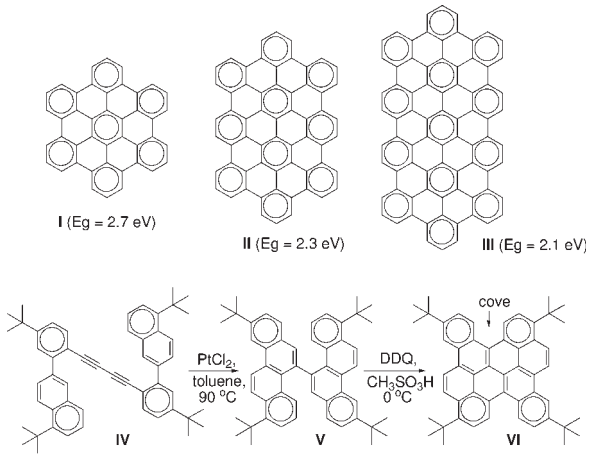

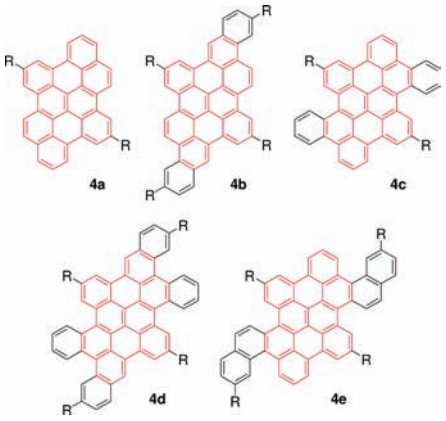

Figure 1. Structure of Targeted PAHs (R = *t*-Bu).

in 71% yield. Species **3a** possesses two nonplanar fjord regions that are subjected to a DDQ-induced oxidative coupling[9] (DDQ = 2,3-dichloro-5,6-dicyanobenzoquinone), giving targeted molecule **4a** in 91% yield. ^{1}H NMR of PAHs **3a** and **4a** in $CDCl_3$ show only nine and seven separate aromatic signals over the range −213−333 K that exhibit no dynamic behavior. For species **3a**, we envisage that an alteration at the fjord chiralty is impeded by a strong steric hindrance.

Table 1 highlights the applicability of this new synthesis to additional bis(biaryl)acetylenes **1b**−**1d**, which delivered extended dibenzochrysene species **3b**−**3d** efficiently through a sequential ICl-cyclization and Mizoroki−Heck coupling. For the resulting **3b** and **3d**, the corresponding DDQ-oxidation in CH_2Cl_2 (0 °C, 6 h) gave the desired PAHs **4b** and **4d** in 79% and 85% yields respectively. Nevertheless, the same DDQ-oxidation of PAH **3c** under the same conditions effected the coupling of only one fjord region, giving compound **4c′** in

(9) DDQ-oxidation: (a) Zhai, L.; Shukla, R.; Rathore, R. *Org. Lett.* **2009**, *11*, 3474. (b) Zhai, L.; Shriya, R.; Wadumethrige, S. H.; Rathore, R. *J. Org. Chem.* **2010**, *75*, 4748.

Scheme 2. Synthetic Route toward Compound **4a** (R = *t*-Bu)

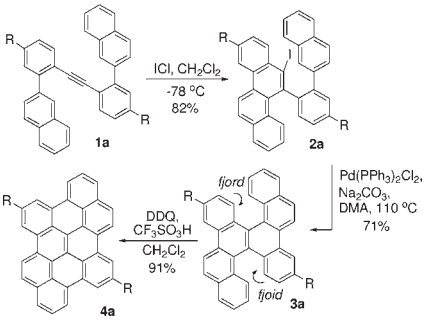

81% yield. To our delight, the second fusion was subsequently achieved with a DDQ-oxidation in a sealed tube at 70 °C (1,2-dichloroethane, 8 h), giving product **4c** in 90% yield.

Scheme 3 depicts the synthesis of large PAH **4e** using dibenzochrysene as the starting building block. Treatment of species **3a** with NBS in $CHCl_3$/DMF produced dibromide derivative **1e** in 88% yield; compound **1e** was subsequently transformed into species **2e** (51% yield) *via* Suzuki

Table 1. A Short Synthesis of PAHs **4b**−**4d** (R = *t*-Bu)

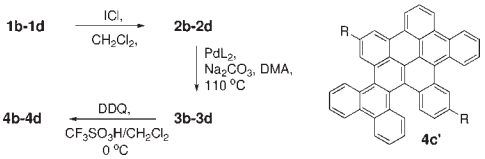

substrate	2 (yields)[a,e]	3 (yields)[b,e]	4 (yields)[c,e]
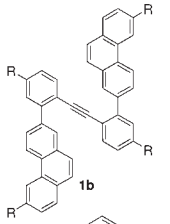 1b	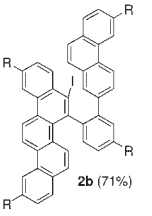 2b (71%)	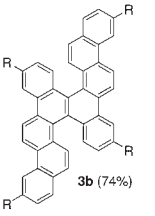 3b (74%)	4b (79%)
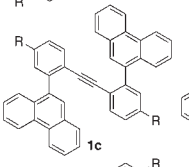 1c	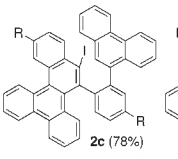 2c (78%)	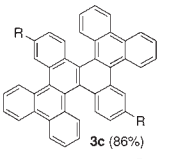 3c (86%)	4c′ (81%) → 4c (90%)[d,e]
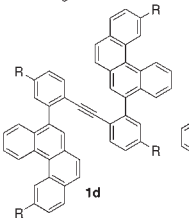 1d	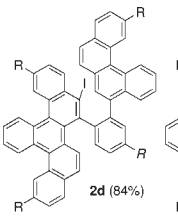 2d (84%)	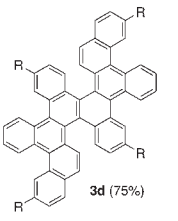 3d (75%)	4d (85%)

[a] ICl (1.1 equiv), CH_2Cl_2, −78 °C. [b] [$Pd(PPh_3)_2Cl_2$] (5 mol %), Na_2CO_3 (4.0 equiv), N,N-dimethylacetamide (0.01 M), 110 °C. [c] DDQ (2.1 equiv), CH_3SO_3H/CH_2Cl_2 (1/10, v/v), 0 °C. [d] DDQ (1.1 equiv), CH_3SO_3H/1,2-dichloroethane (1/10, v/v), 70 °C. [e] Yields are given after purification by column chromatography on silica gel.

Scheme 3. Synthetic Route toward Compounds **4e** (R = *t*-Bu)

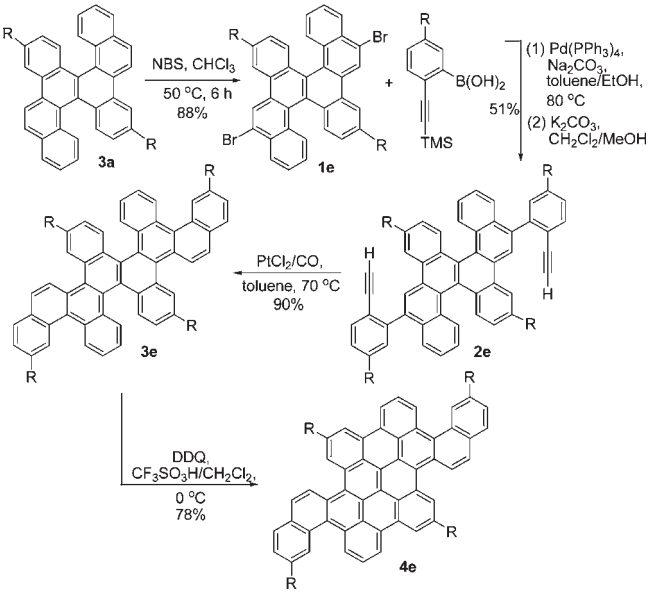

coupling, followed by removal of a silyl group, which subsequently underwent Pt-catalyzed aromatization affording the cyclized product **3e** in 90% yield. For species **3e**, a final DDQ-oxidation enabled a closure of the two fjord regions, giving desired compound **4e** in 78% yield.

The characterization of **3a**–**3e** relies on appropriate analytic methods including elemental analysis, matrix-assisted laser desorption/ionization time-of-flight (MALDI-TOF) high resolution mass spectrometry (HRMS), and ^{1}H and ^{13}C NMR spectra. We obtained single crystals of **3c** for X-ray diffraction.[10] Crystallographic data of its dibenzochrysene precursor **3c** were also acquired to compare their molecular planarity. The unit cells of **3c** and **4c** contain two independent molecules, $Z = 2$. Figure 2 shows the ORTEP drawing for molecule **3c** that reveals a great distortion from planarity in the fjoid geometry, as revealed by a large dihedral angle 77.8° between the **A**–**E**′ and **E**–**A**′ rings. In contrast, the dihedral angle between the **A**/**D** and **A**′/**D**′ benzenes, in the so-called cove areas, is relatively small (51.6°). Species **3c** comprises an S_2 axis with both **A** and **E** rings lying below the **E**′ and **A**′ rings, thus generating a double helicene, defined by rings **E**′–**C**′–**B**′–**B**–**A** and **A**′–**B**′–**B**–**C**–**E** respectively. Notably, the six carbon–carbon distances around the outer rings **A**, **D**, and **E** fall within a narrow range, 1.368–1.416 Å, indicating benzene character. In contrast, we observed large distances (1.60–1.68 Å) for the inner C(1)–C(14), C(2)–C(3), and C(1)–C(15) bonds, near a standard C(sp^2)–C(sp^2) bond (1.467 Å).[11] Accordingly, **3c** is appropriately described by six Clar sextets, with the benzene character located in the six outer rings.

Figure 3 presents an ORTEP drawing of **4c** that confirms our hypothetical structure. The molecular geometry

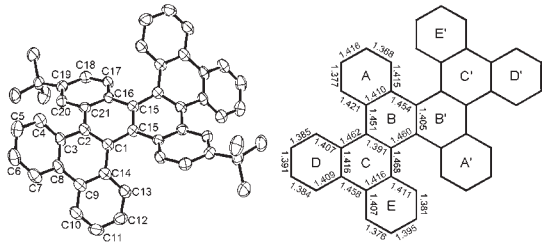

Figure 2. ORTEP drawing of **3c** (left) and bond lengths (right).

is planar, as reflected by the dihedral angle (32.9°) between rings **A** and **D** in the cove region, less than that (51.6°) of molecule **3c**. Species **4c** consists of an S_2 axis with both the **A**′ and **D** rings lying below the **D**′ and **A** rings. Examination of the bond lengths indicates that the inner rings **C**, **F**, **C**′, and **F**′ are unlikely to have Clar sextet character, as evidenced by the two large C(14)–C(15) (1.464 Å) and C(3)–C(4) (1.460 Å) lengths that approximate a standard C(sp^2)–C(sp^2) bond.[11] Molecule **4c** accordingly appears to have six Clar sextets with rings **D** and **E** as two benzene sextets and the **A**/**B** rings representing a naphthalene group.

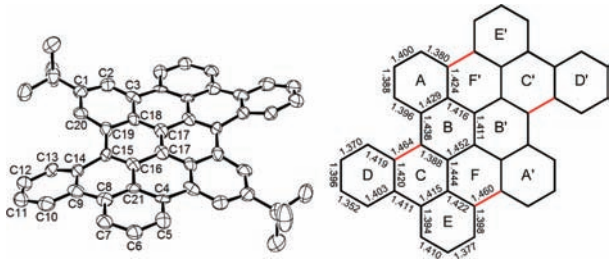

Figure 3. ORTEP drawing of **3d** (left) and bond lengths (right).

Table 2 summarizes the photophysical properties of **3a**–**3e** and **4a**–**4e**. Compounds **3a**–**3e** have the same UV/vis absorption patterns including three maxima in the β-bands (300–360 nm)[12] and two maxima in the *p*-bands (365–460 nm) (Figure 4). Here, we observed bathochromic shifts for the *p*-bands increasing with the array size **3a**→ **3b**/**3c**→ **3d**/**3e**, each with two-benzene alteration. For example, the last maxima of the *p*-bands appear at 375 nm for **3a**, 383/403 nm for **3b**/**3c**, and 409/428 nm for **3d**/**3e**. In the photoluminescence (PL) spectra (Figure s1, Supporting Information (SI)), the emission maxima of **3a**–**3c** are near each other (439–441 nm) but are red-shifted to 453 and 463 nm, respectively, for large arrays **3d** and **3e**.

Of particular interest are the photophysical properties for planar PAHs **4a**–**4e** derived from **3a**–**3e**. As shown

(10) Crystallographic data for compounds **3c** and **4c** are provided in the Supporting Information.

(11) Kveseth, K.; Seip, R.; Kohl, D. A. *Acta Chem. Scand.* **1980**, *A34*, 31.

(12) Discussions of the α-, β-, and *p*-bands of PAHs: (a) Clar, E. *J. Am. Chem. Soc.* **1952**, *62*, 6235. (b) Kastler, M.; Schmidt, J.; Pisula, W.; Sebastiani, D.; Müllen, K. *J. Am. Chem. Soc.* **2006**, *128*, 9526. (c) Karcher, W. *Dibenzanthracenes and Environmental Carcinogenesis*; Cambridge University Press: Cambridge, NY, 1992.

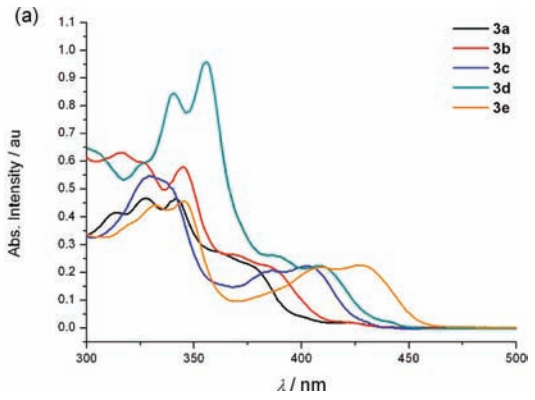

Figure 4. UV/vis absorption spectra of compounds **3a**–**3e**.

in Figure 5, we observed significant bathochromic shifts for the absorption maxima of **4a**–**4e** in both β-bands and the *para*-band relative to those of **3a**–**3e**. For example, the last maxima of their *p*-bands are shifted to larger wavelengths up to 86–103 nm. Large bathochromic shifts (50–74 nm) were also observed for the PL spectra of species **4a**–**4e** (Figure s2, SI) relative to those of **3a**–**3e**. Figures 5 and s2 also reveal gradual bathochromic shifts in the last absorption maxima (478–519 nm), as well as the emission maxima (491–537 nm), with increasing sizes **4a**→ **4b/4c**→ **4d/4e** (see Table 2). This information reveals that the increasing array size on such planar skeletons significantly affects both UV and PL wavelengths.

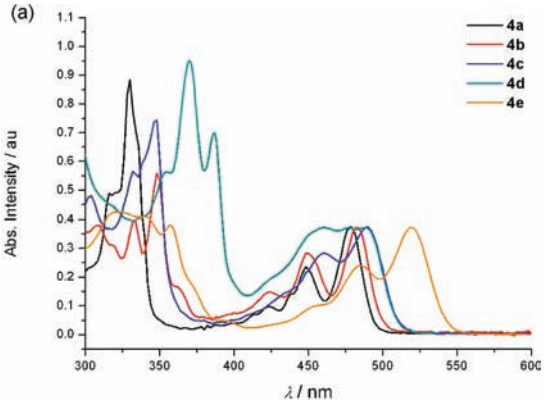

Figure 5. UV/vis absorption spectra of compounds **4a**–**4e**.

According to cyclic voltammetry (Figure s3, SI), species **3a**–**3e** show one reversible oxidation (0.75–0.93 V vs Ag^+/Ag) due to a simultaneous oxidation of two nonplanar half sizes whereas planar PAHs **4a**–**4e** reveal two reversible oxidations. For small PAHs **4a**–**4c**, the two oxidation potentials (0.52–0.54, 0.68–0.71 V), given from the successive oxidation of the two half arrays, are close to each other but recognizable. Large array sizes **4d**–**4e** have two well separated oxidation potentials (0.66–0.70, 1.08–1.17 V); the first oxidation is assigned to a simultaneous oxidation of two half arrays. We estimated the HOMO energy levels from the UV/vis spectra. As shown in Table 2, the electron delocalization of nonplanar **3a**–**3e** appears to be less efficient because variations of their energy gaps (E_g) are small, within a small range (2.84–2.71 eV). In contrast, a significant decrease in the E_g values is shown for planar PAHs **4a**–**4e**, within a reasonable range (2.51–2.27 eV). Notably, species **4c** bearing two cove regions has E_g = 2.42 eV which is even smaller than that of planar **4b** (E_g = 2.48 eV) that lacks a cove region. For species **4d** and **4e** bearing four cove regions, their energy gaps are distinct, 2.42 vs 2.27 eV. These observations reveal that large planar PAHs are not the decisive factor to obtain small E_g among various geometric isomers.

Table 2. Optical and Electrochemical Data

PAHs	Abs_{max} (nm)[a]	PL (nm)[b]	HOMO (eV)[c]	LUMO (eV)[d]	E_g (eV)[e]	Φ[b,f]
3a	313, 327, 342, 362, 375	441	−5.54	−2.70	2.84	0.12
3b	316, 326, 345, 369, 383	442	−5.51	−2.67	2.84	0.33
3c	329, 337, 386, 403	439	−5.47	−2.63	2.84	0.20
3d	326, 340, 356, 387, 409	453	−5.44	−2.67	2.77	0.18
3e	332, 345, 407, 428	463	−5.40	−2.69	2.71	0.40
4a	316, 330, 424, 448, 478	491	−5.13	−2.62	2.51	0.61
4b	332, 348, 424, 449, 482	498	−5.07	−2.59	2.48	0.49
4c	332, 348, 432, 460, 489	506	−5.12	−2.70	2.42	0.17
4d	354, 370, 387, 458, 477, 489	509	−5.20	−2.78	2.42	0.38
4e	321, 341, 357, 454, 484, 519	537	−5.28	−3.01	2.27	0.21

[a] 10^{-5} M in CH_2Cl_2. [b] 10^{-6} M in CH_2Cl_2. [c] HOMO was calculated from the oxidation potential of CV. [d] LUMO was calculated by the sum of HOMO and E_g. [e] Calculated from the UV/vis absorption. [f] Coumarin 1 as the standard.

In summary, we have developed a new synthesis of large PAHs with low Clar sextets. This synthesis involves initial bis(biaryl)acetylene **1**, which undergoes initial ICl-aromatization and a subsequent Mizoroki–Heck coupling reactions to give dibenzochrysene derivatives **3** that can be transformed into planar PAH **4** using DDQ-oxidation. X-ray diffraction studies reveal highly nonplanar skeleta for dibenzochrysene species **3c**, but a planar geometry for PAHs **4c**. The photophysical properties of **4a**–**4e** including UV/vis, photoluminscence, and cyclic voltammetry indicate that these properties are greatly affected by the increasing array size, whereas those of nonplanar **3a**–**3e** appear to be less sensitive to such size variations.

Acknowledgment. We thank National Science Council, Taiwan, for financial support of this work.

Supporting Information Available. Spectral data, NMR spectra, MALDI-Mass, PL, CV measurements of new compounds, and X-ray crystallographic data of compounds **3c** and **4c** are provided in Supporting Information. This materials is available free of charge via the Internet at http://pubs.acs.org.